Khang Hoang,^{1,*} Camille Latouche,² and Stéphane Jobic²

¹Center for Computationally Assisted Science and Technology & Department of Physics, North Dakota State University, Fargo, North Dakota 58108, United States ²Institut des Matériaux Jean Rouxel (IMN), Université de Nantes, CNRS, 2 rue de la Houssinière, 44322 Nantes, France (Dated: February 21, 2022)

Rare-earth doped barium zirconate (BaZrO₃) ceramics are of interest as proton-conducting and luminescent materials. Here, we report a study of dysprosium (Dy) and other relevant point defects in BaZrO₃ using hybrid density-functional defect calculations. The tetravalent Dy⁴⁺ is found to be structurally and electronically stable at the Zr lattice site (i.e., as Dy_{Zr}), but most often energetically less favorable than the trivalent Dy³⁺ (i.e., Dy_{Zr}) in as-synthesized BaZrO₃, due to the formation of low-energy, positively charged oxygen vacancies and the mixed-site occupancy of Dy in the host lattice. The Dy⁴⁺/Dy³⁺ ratio can, in principle, be increased by preparing the material under highly oxidizing and Ba-rich conditions and co-doping with acceptor-like impurities; however, post-synthesis treatment may still be needed to realize a non-negligible Dy⁴⁺ concentration. We also find that certain unoccupied Dy 4f states and the O 2p states are strongly hybridized, a feature not often seen in rare-earth-containing materials, and that the isolated Dy_{Zr} defect might be the source of a broad blue emission in band-to-defect ("charge-transfer") luminescence.

I. INTRODUCTION

Dysprosium (Dy) is very stable as the trivalent Dy³⁺ in solid compounds, yet the divalent Dy²⁺ has also been observed in some fluorides [1, 2] and suspected to be photogenerated under irradiation in persistent luminescent phosphors [3]. The tetravalent Dy⁴⁺ was almost unknown up to very recently [4-6]. Han et al. [4] was the first to claim experimental evidence of Dy⁴⁺ in BaZrO₃, a perovskite structure type host lattice commonly investigated for its proton conductivity ability [7]. Subsequent reports provided further evidence for the presence of the tetravalent state in samples prepared in oxidizing atmospheres [5, 6] and the mixed-site occupancy of Dy in the host lattice [8], and discussed the possible role of Dy⁴⁺ as a charge-compensating defect in the oxidation reaction [5, 6]. The stability of Dy⁴⁺ is thus of interest because of not just the exotic valence state but also the implication it has for defect-related processes in the material.

On the theory side, the interaction between the Dy dopant and BaZrO₃, including native point defects and other impurities that may be present in the host material, has not been investigated, and thus a theoretical foundation for understanding the experimental observations is still lacking. First-principles defect calculations [9] based on a hybrid density-functional theory (DFT)/Hartree-Fock approach [10] can provide a detailed understanding of the atomic and electronic structure (including the oxidation state), energetics, and optical properties of rare-earth (RE) dopants in solid compounds [11, 12].

Here, we present an investigation of Dy and other relevant defects in BaZrO₃ using hybrid density-functional defect calculations. Explicit calculations are carried out

for native point defects and substitutional Dy and yttrium (Y) impurities. Based on the results, we discuss the stability of $\mathrm{Dy^{3+}}$ and $\mathrm{Dy^{4+}}$ and the tuning of the $\mathrm{Dy^{4+}}/\mathrm{Dy^{3+}}$ ratio and the lattice site preference via tailoring the synthesis conditions and co-doping, or via postsynthesis treatment. Possible band-to-defect and defect-to-band (also known as "charge-transfer") optical transitions involving the isolated $\mathrm{Dy_{Zr}}$ defect are also explored.

II. METHODOLOGY

Defects in BaZrO₃ are modeled using a supercell approach in which a defect is included in a periodically repeated finite volume of the host material. Here, the term "defect" is referred generally to either native point defects or impurities, i.e., extrinsic defects, intentionally added (i.e., dopants) or unintentionally present in the material. A defect is characterized by its formation energy. Defects with a lower formation energy will be more likely to form and occur with a higher concentration.

The formation energy of a defect X in effective charge state q (with respect to the host lattice) is defined as [9]

$$E^{f}(\mathbf{X}^{q}) = E_{\text{tot}}(\mathbf{X}^{q}) - E_{\text{tot}}(\text{bulk}) - \sum_{i} n_{i}\mu_{i} \qquad (1)$$
$$+ q(E_{v} + \mu_{e}) + \Delta^{q},$$

where $E_{\text{tot}}(\mathbf{X}^q)$ and $E_{\text{tot}}(\text{bulk})$ are the total energies of the defect-containing and bulk (i.e., perfect and undoped) supercells; n_i is the number of atoms of species i that have been added $(n_i > 0)$ or removed $(n_i < 0)$ to form the defect; μ_i is the atomic chemical potential, representing the energy of the reservoir with which atoms are being exchanged. μ_e is the electronic chemical potential, i.e., the Fermi level, representing the energy of the electron reservoir, referenced to the valence-band maximum

^{*} Corresponding author. E-mail: khang.hoang@ndsu.edu

(VBM) in the bulk $(E_{\rm v})$. Finally, Δ^q is the correction term to align the electrostatic potentials of the bulk and defect supercells and to account for finite-size effects on the total energy of charged defects [13, 14].

From the defect formation energy, one can determine the thermodynamic transition level between charge states q and q' of a defect, $\epsilon(q/q')$ (q>q'), defined as the Fermilevel position at which the formation energy of the defect in charge state q is equal to that in state q'. This level [also referred to as the (q/q') level], corresponding to a defect level, would be observed in experiments where the defect in the final charge state q' fully relaxes to its equilibrium configuration after the transition. The optical transition level $E_{\rm opt}^{q/q'}$, on the other hand, is defined similarly but with the total energy of the final state q' (q) calculated using the lattice configuration of the initial state q (q') for the absorption (emission) process [9].

The total-energy electronic structure calculations are based on DFT with the Heyd-Scuseria-Ernzerhof (HSE) functional [10], the projector augmented wave method [15], and a plane-wave basis set, as implemented in the Vienna Ab Initio Simulation Package (VASP) [16]. The Hartree-Fock mixing parameter and the screening length are set to the default values of 0.25 and 10 Å, respectively. We use the PAW potentials in the VASP database which treat Ba $5s^25p^66s^2$, Zr $4s^24p^65s^24d^2$, O $2s^22p^4$, Dy $5s^25p^64f^{10}6s^2$, and Y $4s^24p^65s^24d^1$ explicitly as valence electrons and the rest as core electrons. Defects are simulated using a cubic 40-atom supercell and a $2\times2\times2$ Monkhorst-Pack k-point mesh for the integrations over the Brillouin zone. In the defect calculations, the lattice parameters are fixed to the calculated bulk values but all the internal coordinates are relaxed. In all the calculations, the energy cutoff is set to 500 eV and spin polarization is included; structural relaxations are performed with HSE and the force threshold is chosen to be 0.01 eV/Å. The DFT+U method [17], with $U^{\text{eff}} = 6.0 \text{ eV}$ applied on the Dy 4f states, is also employed to calculate the electronic structure of Dy-doped BaZrO₃, and the result is compared with that from the HSE calculations (see Sec. IIIB). For a detailed discussion of the suitability of the hybrid DFT/Hartree-Fock approach to the study of defect physics in RE-doped materials, in comparison with other methods such as DFT and DFT+U, see Ref. 12.

The chemical potentials of Ba, Zr, Dy, Y, and O are referenced to the total energy per atom of bulk Ba, Zr, Dy, Y, and O_2 at 0 K, respectively. $\mu_{\rm Ba}$, $\mu_{\rm Zr}$, and $\mu_{\rm O}$ vary over a range determined by the formation enthalpy of BaZrO₃ such that $\mu_{\rm Ba} + \mu_{\rm Zr} + 3\mu_{\rm O} = \Delta H({\rm BaZrO_3})$ (calculated to be $-17.29~{\rm eV}$ at 0 K). We examine defect landscape in BaZrO₃ in two limits: (i) the (Ba,O)-rich condition where the host material is assumed to be in thermodynamic equilibrium with BaO ($\Delta H = -5.09~{\rm eV}$) and O₂ gas at 1 atm, and (ii) the (Zr,O)-rich condition where equilibrium with ZrO₂ ($\Delta H = -10.99~{\rm eV}$) and O₂ gas at 1 atm is assumed. The temperature range from 1000°C to 1600°C is often used in the preparation of Dy-doped BaZrO₃ samples [4–6, 8]. Under the mentioned condi-

tions, $\mu_{\rm O}$ is -1.45 eV (at $1000^{\circ}{\rm C}$) or -2.56 eV ($1600^{\circ}{\rm C}$) [18]. The specific value of $\mu_{\rm Dy}$ and $\mu_{\rm Y}$ is obtained by assuming equilibrium with Dy₂O₃ ($\Delta H = -18.53$ eV) and Y₂O₃ ($\Delta H = -19.00$ eV), respectively.

In the above, we explicitly take into account the temperature and pressure dependence when considering gasphase species, specifically when calculating the oxygen chemical potential (which is related to the Gibbs free energy of O_2 gas at temperatures and oxygen partial pressures under consideration) [19]. Temperature and pressure effects are usually small for solid phases and thus can be ignored; besides, significant cancellation occurs between different terms in the defect formation energy and when comparing different defects [9]. Also note that the defect transition levels, $\epsilon(q/q')$ and $E_{\rm opt}^{q/q'}$, are independent of the choice of the atomic chemical potentials.

It should be realized that the sets of the chemical potentials determined from the above assumptions are relevant to the system during synthesis, when *all* the constituent elements of the host compound are in exchange with their respective reservoirs. The experimental conditions during, e.g., post-synthesis treatment, measurement, or use are often very different, according to which only certain element(s) of the host may be exchanged with the environment. These conditions, if known, can be translated into other sets of the chemical potentials. For further discussion with examples of defect landscape in different experimental situations in other classes of materials and physical phenomena, see Refs. 20 and 21.

III. RESULTS AND DISCUSSION

A. Bulk properties and native defects

In bulk (cubic) BaZrO₃, the calculated lattice constant is 4.200 Å, compared to 4.192 Å in experiments [22]. The calculated band gap is 4.68 eV, an indirect gap with the VBM at the $R(\frac{1}{2}, \frac{1}{2}, \frac{1}{2})$ point in the reciprocal space and the conduction-band minimum (CBM) at the Γ (0,0,0) point. For comparison, the reported experimental band gap varies in the range from 4.0 eV to 5.3 eV [23–25]. The electronic contribution to the static dielectric constant is found to be 3.98 in our HSE calculations, based on the real part of the dielectric function $\epsilon_1(\omega)$ for $\omega \to 0$. The ionic contribution is calculated using density-functional perturbation theory [26], within the generalized-gradient approximation [27]. The total dielectric constant is 51.75, in good agreement with the reported experimental value of \sim 47 at 0 K (or \sim 52 if taking into account the porosity of the sample [28]). In a simple ionic model, BaZrO₃ can be regarded as consisting of Ba^{2+} , Zr^{4+} , and O^{2-} .

Figure 1 shows the formation energy of selected native point defects in BaZrO₃. The dominant defects are positively charged oxygen vacancy, $V_{\rm O}^{2+}$ (or, equivalently, the removal of an O²⁻ ion from the host material), and negatively charged barium vacancy, $V_{\rm Ba}^{2-}$ (the removal of a Ba²⁺ from the host). In the absence of impurities, in-

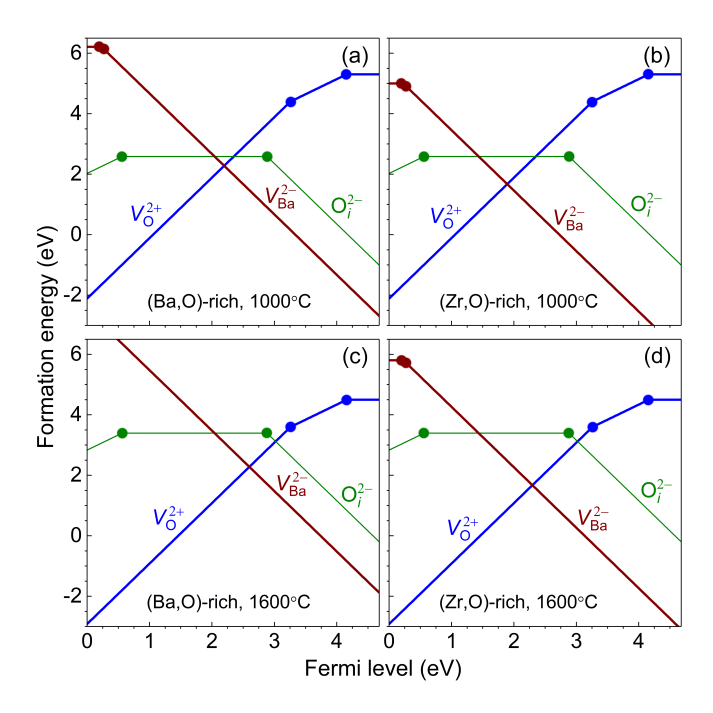


FIG. 1. Formation energies of selected native defects in $BaZrO_3$ as a function of the Fermi level from the VBM (at 0 eV) to the CBM (4.68 eV), under the (Ba,O)-rich or (Zr,O)-rich condition at 1000° C or 1600° C. Only segments of the energy line corresponding to the lowest-energy charge states are shown. The slope of these segments indicates the charge state (q): positively (negatively) charged defect configurations have positive (negative) slopes; horizontal segments correspond to neutral configurations. Large solid dots connecting two segments with different slopes mark the defect levels.

tentionally incorporated or unintentionally present, the Fermi level is "pinned" at the position where $V_{\rm O}^{2+}$ and $V_{\rm Ba}^{2-}$ have equal formation energies and hence charge neutrality is maintained. Other defects, such as the oxygen interstitial $({\rm O}_i)$, have a higher formation energy. In ${\rm O}_i$, the extra O combines with one of the O atoms of the host to form an O–O dumbbell that is perpendicular to the line connecting the two Ba atoms in the original Ba–O–Ba chain. Our results for the native defects are in agreement with those reported by Rowberg et al. [29], except that we find a lower-energy configuration for ${\rm O}_i^0$.

B. Doping with dysprosium

Figure 2 shows the formation energy of the substitutional Dy impurity either at the Ba site (Dy_{Ba}) or the Zr site (Dy_{Zr}) . We find that Dy_{Ba} is stable only as Dy_{Ba}^+ (i.e., the trivalent Dy^{3+} at the Ba site, with spin S=5/2), irrespective of the chosen set of chemical potentials (which represents synthesis conditions). In the Dy_{Ba}^+ configuration, the Dy^{3+} ion moves off-center by 0.69 Å and comes closer to six of its twelve neighboring O atoms, with the Dy-O bond length being 2.277-2.512

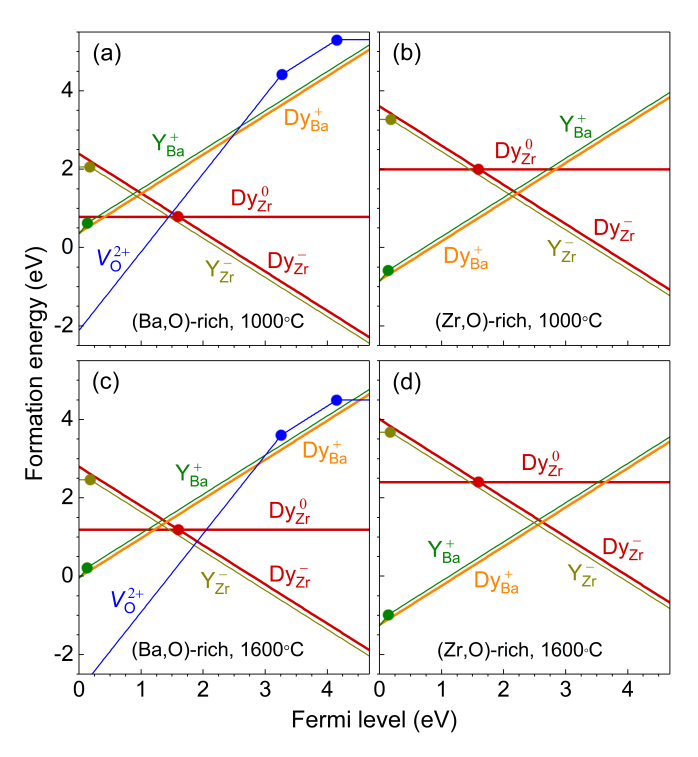


FIG. 2. Formation energies of Dy- and Y-related defects as a function of the Fermi level from the VBM to the CBM, under the (Ba,O)-rich or (Zr,O)-rich conditions. Large solid dots mark the defect levels. The results for $V_{\rm O}$ under the (Ba,O)-rich condition are repeated here for easy comparison.

Å. $\mathrm{Dy_{Zr}}$ is, on the other hand, structurally and electronically stable as $\mathrm{Dy_{Zr}}$ (i.e., the trivalent $\mathrm{Dy^{3+}}$ at the Zr site, S=5/2) and $\mathrm{Dy_{Zr}}^0$ (i.e., the tetravalent $\mathrm{Dy^{4+}}$ at the Zr site, S=3). The thermodynamic transition level (0/-) of $\mathrm{Dy_{Zr}}$ is at 1.61 eV above the VBM; i.e., above (below) this level, $\mathrm{Dy^{3+}}$ ($\mathrm{Dy^{4+}}$) is energetically more stable (see further discussion later). In the $\mathrm{Dy_{Zr}}^0$ ($\mathrm{Dy_{Zr}}^-$) configuration, the Dy–O bond is 2.131–2.134 Å (2.188 Å), consistent with the fact that the ionic radius of $\mathrm{Dy^{4+}}$ (0.78 Å) [30] is smaller than that of $\mathrm{Dy^{3+}}$ (0.912 Å) [31].

To understand the electronic stability of Dy^{3+} and Dy^{4+} , we show in Fig. 3 the total and $\mathrm{Dy}\ 4f$ -projected electronic density of states (DOS) of Dy-doped BaZrO₃. In the DOS calculations, one Zr atom in the 40-atom BaZrO₃ supercell is substituted with Dy; i.e., the chemical composition is Ba₈DyZr₇O₂₄, which corresponds to the Dy_{Zr}^0 defect configuration discussed earlier. Highquality DOS is achieved by using a Γ -centered $4\times4\times4$ k-point mesh. The ground state of Dy⁴⁺ is $4f^8$. In the calculated DOS, we find that Dy introduces seven spin-up occupied 4f states at about -9 eV, one spin-down occupied 4f state at about -0.7 eV (not clearly seen in Fig. 3 due to the energy resolution of the calculation but is confirmed by electron counting and by an examination of the wave functions), and six spin-down unoccupied 4f states in the host band gap (at about +2.5 eV and +3.2 eV). In going from $\mathrm{Dy_{Zr}^0}$ to $\mathrm{Dy_{Zr}^-}$, the lowest unoccupied Dy

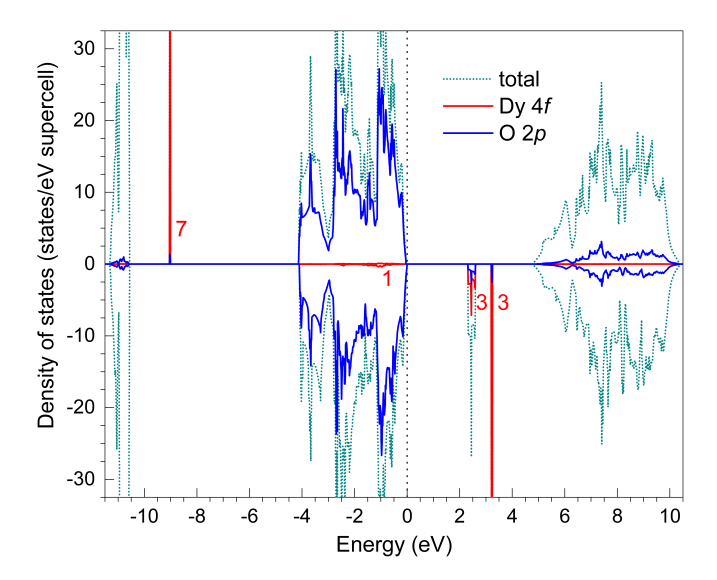


FIG. 3. Total and projected densities of states (DOS) of Dydoped BaZrO₃, specifically $\mathrm{Dy}_{\mathrm{Zr}}^0$, obtained in HSE calculations. The spin-majority spectrum is on the +y axis, and the spin-minority spectrum is on the -y axis. The number of 4f electrons at the Dy 4f-projected DOS peaks is indicated. The zero of energy is set to the highest occupied state.

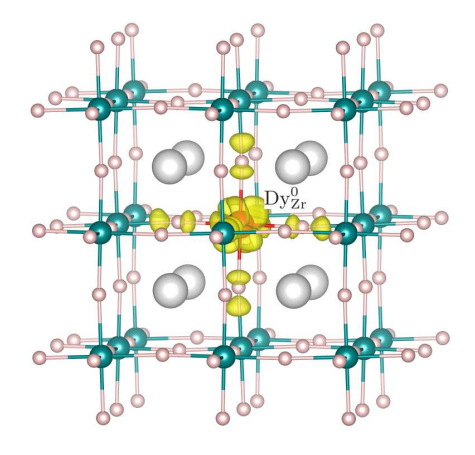


FIG. 4. Structure of the $\mathrm{Dy}_{\mathrm{Zr}}^0$ (i.e., Dy^{4+}) defect configuration in BaZrO_3 . The charge density shows an electron hole localized at the Dy ion and the neighboring O sites. The isovalue for the charge-density isosurface (yellow) is set to 0.02 $e/\mathring{\mathrm{A}}^3$. The large (gray) spheres are Ba, medium (red/blue) spheres are Dy/Zr, and small (red) spheres are O.

4f state captures an electron and Dy^{4+} becomes Dy^{3+} $(4f^9)$. Note that our DFT+U calculations produce an electronic structure that is qualitatively similar to that reported in Fig. 3. However, since the Hubbard U term is only applied on the Dy 4f states and all other orbitals in the compound are left uncorrected, the host DFT+U band gap is significantly underestimated. As a result, the position of the Dy 4f states with respect to the band edges are different from that obtained with HSE.

Although the RE 4f orbitals are often regarded as being well shielded by the outer $5s^2$ and $5p^6$ electron shells

and thus contribute very weakly to chemical bonding, we find a strong hybridization between certain unoccupied Dy 4f orbitals and the O 2p states. This can be observed in the relatively broad peak at about +2.5 eV in the calculated DOS shown in Fig. 3 where there are contributions from the O 2p states and the structure of the O 2p-derived DOS peak resembles that of the Dy 4f-derived one. Figure 4 shows the lattice geometry of Dy $_{\rm Zr}^0$ and the charge density of the associated electron hole (with respect to Dy $_{\rm Zr}^-$). The charge density, again, shows a strong Dy 4f-O 2p hybridization. Note that the mixing of the RE 4f states and the O states has also been reported in the case of Gd₃Ga₅O₁₂ [32].

It should be noted that the Dy-derived peaks in the DOS (Fig. 3) are not defect levels associated with $\mathrm{Dy_{Zr}}$. Indeed, those Kohn-Sham levels cannot directly be identified with any levels that can be observed in experiments [9]. The (0/-) level of $\mathrm{Dy_{Zr}}$, for example, must be calculated using the total energies of the $\mathrm{Dy_{Zr}}^0$ and $\mathrm{Dy_{Zr}}^0$ configurations as described earlier and reported in Fig. 2.

Considering only the Dy-related defects, we find that, under the (Zr,O)-rich condition, Dy^{3+} (in the form of $\mathrm{Dy}^+_{\mathrm{Ba}}$ and/or $\mathrm{Dy}^-_{\mathrm{Zr}}$) is energetically more favorable than Dy^{4+} (in the form of $\mathrm{Dy}^0_{\mathrm{Zr}}$) in the entire range of Fermilevel values; see Figs. 2(b) and 2(d). Under the (Ba,O)-rich condition, Dy^{4+} is energetically more favorable than Dy^{3+} in a small range of Fermi-level values, and this range is greater at lower temperatures; see Figs. 2(a) and 2(c). This is because the lower temperature leads to higher formation energies of V_{O}^{2+} and $\mathrm{Dy}^+_{\mathrm{Ba}}$ and lower formation energies of $\mathrm{Dy}^0_{\mathrm{Zr}}$ (as well as $\mathrm{Dy}^-_{\mathrm{Zr}}$), thus increasing the range of Fermi-level values in which $\mathrm{Dy}^0_{\mathrm{Zr}}$ is energetically more favorable; the formation energy of $\mathrm{Dy}^0_{\mathrm{Zr}}$ is 0.78 eV at 1000°C, compared to 1.19 eV at 1600°C.

That Dy⁴⁺-favorable range, however, may not even be accessible if one takes into consideration the native defects. Under the (Ba,O)-rich condition at 1600°C, for example, the Fermi level is at 1.90 eV, determined predominantly by $V_{\rm O}^{2+}$ and ${\rm Dy}_{\rm Zr}^-$, at which the formation energy of ${\rm Dy}_{\rm Zr}^0$ is higher than that of ${\rm Dy}_{\rm Zr}^-$ by 0.30 eV; see Fig. 2(c). Only at lower temperatures, e.g., 1000°C, ${\rm Dy}_{\rm Zr}^0$ has a lower energy than ${\rm Dy}_{\rm Zr}^-$ (by 0.11 eV, where the Fermi level is at 1.50 eV); see Fig. 2(a). Note, however, that an energy difference of ~0.1 eV is within the error bar of our calculations. Yet what is clear here is that low-energy, positively charged defects, e.g., $V_{\rm O}^{2+}$ and ${\rm Dy}_{\rm Ba}^+$, reduce the ${\rm Dy}^{4+}$ -favorable range or make it inaccessible. The effect of Y co-doping will be discussed later.

Overall, our results indicate that higher $\mathrm{Dy^{4+}}$ concentrations might be achieved with higher oxygen (μ_{O}) and barium (μ_{Ba}) chemical potential values [and hence lower zirconium (μ_{Zr}) chemical potential values]. Higher μ_{O} values represent more oxidizing environments, which are usually associated with oxygen gas at lower temperatures and higher oxygen partial pressures [19], and lead to a reduced oxygen vacancy concentration (particularly, that of V_{O}^{2+}) due to an increase in the defect's formation energy. Similarly, higher μ_{Ba} values, which can be achieved

by preparing the material under Ba-rich conditions, result in a reduction or suppression of the Ba-site occupancy (the formation of $\mathrm{Dy_{Ba}^{+}}$). Lower μ_{Zr} values result in a lower formation energy (and hence a higher concentration) of Dy at the Zr site. Note that our argumentation assumes that the material is prepared under (or close to) thermodynamic equilibrium conditions. It is, however, not clear at this point if the defect landscape reported in Fig. 2(a) or others that are close to it can be realized under actual synthesis conditions such that the $\mathrm{Dy^{4+}}$ concentration is significant, or if post-synthesis treatment is needed to realize $\mathrm{Dy^{4+}}$ (see more below).

The above results showing Dy_{Ba} can have a low formation energy are consistent with experimental reports of the mixed-site occupancy in which Dy is incorporated at both the Ba and Zr sites [8]. The synthesis conditions in Han et al. [8] should be somewhere between the (Ba,O)-rich and (Zr,O)-rich limits discussed in this work.

C. (Co-)doping with yttrium

To understand the effects of doping or co-doping with Y, calculations are also carried out for the substitutional Y impurity. Figure 2 shows that Y_{Ba} is most stable as Y_{Ba}^+ (i.e., Y^{3+} at the Ba site, S=0), except in a very small range of Fermi-level values near the VBM (0 to 0.15eV) where it is stable as Y_{Ba}^{2+} that is, in fact, a complex of Y_{Ba}^{+} and a localized hole at an O site (i.e., O^{-}); the Y^{3+} ion in the Y_{Ba} defects is significantly off-center (by 0.73 Å in the case of Y_{Ba}^+), similar to Yb_{Ba} . Y_{Zr} introduces a defect level, (0/-), at 0.18 eV above the VBM; and the extra electron in Y_{Ba}^0 is localized over several neighboring O sites. Like Dy, Y can thus be incorporated at the Zr site and/or the Ba site, depending on the Fermi-level position, which is consistent with the mixed-site occupancy observed in experiments [33–35]. Our results for Y are similar those reported by Rowberg et al. [29].

When Y is incorporated at the Zr lattice site (thus forming the Y_{Zr}^- defect) with a concentration higher (i.e., a formation energy lower) than that of Dy_{Zr}^- , as it is the case shown in Fig. 2, the Fermi level will be shifted toward the VBM as the system reestablishes charge neutrality. Under the (Ba,O)-rich condition, for example, the Fermi level is now determined predominantly by $V_{\rm O}^{2+}$ and Y_{Zr}^- ; see Figs. 2(a) and 2(c). As the Fermi level is shifted leftward, the formation energy of Dy_{Zr} increases (and hence its concentration decreases) whereas that of Dy_{Zr}^0 remains constant, thus increasing the Dy^{4+}/Dy^{3+} ratio. Any acceptor-like defect that shifts the Fermi level would lead to a similar effect. For instance, Rb_{Ba} and Sc_{Zr} , stable as $\mathrm{Rb}_{\mathrm{Ba}}^-$ and $\mathrm{Sc}_{\mathrm{Zr}}^-$, respectively, as reported in Ref. 29, would be effective if incorporated with a concentration higher than that of Dy_{Zr}^- ; for an illustration of the Fermilevel shifting effect, see, e.g., Fig. 11(a) of Ref. 20. Note that, even with co-doping, one still need to suppress the formation of oxygen vacancies and the Ba-site occupancy (see above), otherwise $V_{\rm O}^{2+}$ and/or Dy_{Ba} will counteract the effect of co-doping. Also note that, a Fermi-level shift alone (i.e., without decreasing the formation energy of $\mathrm{Dy}_{\mathrm{Zr}}^0$) does not increase the Dy^{4+} concentration as $\mathrm{Dy}_{\mathrm{Zr}}^0$ is a neutral defect and its formation energy is independent of the Fermi-level position; i.e., it only changes the Dy^{3+} concentration and thus the $\mathrm{Dy}^{4+}/\mathrm{Dy}^{3+}$ ratio.

D. Post-synthesis treatment

Given the above results and discussion, one may expect that Dy exists entirely or predominantly as the trivalent Dy^{3+} (i.e., $\mathrm{Dy}_{\mathrm{Zr}}^{-}$) in $\mathrm{BaZrO_3}$ under normal synthesis conditions, and $\mathrm{Dy}_{\mathrm{Zr}}^{-}$ is charge-compensated predominantly by V_{O}^{2+} and/or $\mathrm{Dy}_{\mathrm{Ba}}^{+}$. The native defects and RE-related defects, once formed or incorporated during the synthesis reaction, are expected to remain trapped in the material after the synthesis and act as athermal, prexisting defects in subsequent experiments [20]. We refer to the $\mathrm{BaZrO_3}$ material at this stage as being as-synthesized.

Upon heat treating as-synthesized BaZrO₃ in oxidizing atmospheres, the following reaction is expected:

$$\frac{1}{2}O_2 + V_{O}^{2+} + 2Dy_{Zr}^{-} \to O_{O}^{0} + 2Dy_{Zr}^{0},$$
 (2)

in which oxygen from the environment fills the oxygen vacancies and, to maintain charge neutrality, Dy^{3+} (i.e., $\mathrm{Dy}^{-}_{\mathrm{Zr}}$) is oxidized to Dy^{4+} (i.e., $\mathrm{Dy}^{0}_{\mathrm{Zr}}$). Here, we assume that the system exchanges only oxygen with the environment. It should be emphasized here that reaction (2) is possible because Dy^{4+} (and Dy^{3+}) can be stabilized in BaZrO_3 , even when Dy^{4+} is not already present in as-synthesized samples. Also note that, in principle, the right-hand side of Eq. (2) can include $\mathrm{Dy}^{-}_{\mathrm{Zr}}$ and an electron hole localized at an O site ("O–") or a free hole (h^+) which acts as a charge-compensating defect; however, we find that neither O– nor h^+ can be stabilized when an electron hole is added to the supercell containing $\mathrm{Dy}^{-}_{\mathrm{Zr}}$.

The above oxidation reaction may explain the presence of the tetravalent Dy⁴⁺ reported in BaZrO₃-based materials prepared in highly oxidizing atmospheres [4–6]. It would be useful if the Dy⁴⁺/Dy³⁺ ratio and the Fermi-level position of those samples can be determined.

As reported by Han et al. [4], Dy⁴⁺ can be converted into Dy³⁺ again in subsequent heat treatment in highly reducing atmospheres (e.g., H₂). Using our defect notation, the reaction can be written as

$$O_{O}^{0} + H_{2} + 2Dy_{Zr}^{0} \rightarrow H_{2}O + V_{O}^{2+} + 2Dy_{Zr}^{-}.$$
 (3)

Again, this reaction, like reaction (2), is possible because both Dy^{3+} and Dy^{4+} can be stabilized in BaZrO₃.

E. Band-to-defect luminescence

Finally, we examine optical transitions involving the isolated $\rm Dy_{Zr}$ defect in $\rm BaZrO_3$. Given the presence of

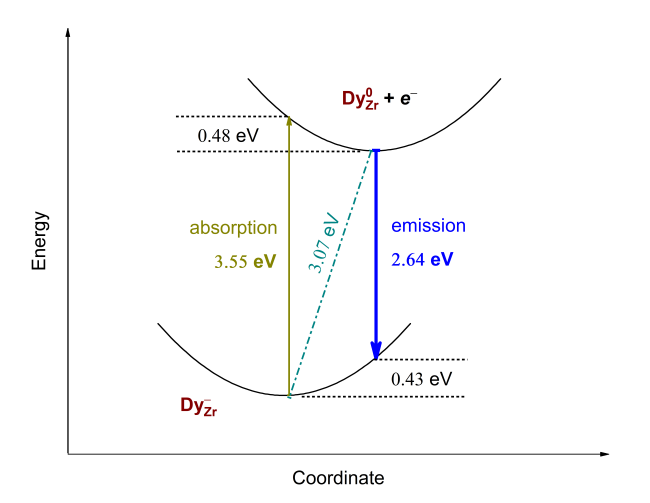


FIG. 5. Configuration-coordinate diagram illustrating optical emission (down arrow) and absorption (up arrow) processes involving $\mathrm{Dy_{Zr}}$ in $\mathrm{BaZrO_3}$. The thermal energy [also called the zero-phonon line (ZPL), the dash-dotted line] is the thermodynamic transition level $\epsilon(0/-)$ relative to CBM. The values sandwiched between two dotted lines are the relaxation energies (the Franck-Condon shifts). Axes are not to scale. For a detailed discussion of the configuration-coordinate diagram representation, see, e.g., Alkauskas et al. [36].

the (0/-) level in the host band gap, Dy_{Zr} may act as a carrier trap for band-to-defect and defect-to-band optical transitions. Figure 5 illustrates Dy_{Zr}-related optical absorption and emission processes. Under illumination, for example, the $\mathrm{Dy}_\mathrm{Zr}^-$ defect configuration can absorb a photon and become Dy_{Zr}^0 with the removed electron being excited into the conduction band. The peak absorption energy related to the optical transition level $E_{\rm opt}^{-/0}$ (the formation energy difference between $\mathrm{Dy}_{\mathrm{Zr}}^-$ and the $\mathrm{Dy}_{\mathrm{Zr}}^0$ configuration in the lattice geometry of Dy_{Zr}^-) is 3.55 eV, with a relaxation energy (i.e., the Franck-Condon shift) of 0.48 eV. Dy⁰_{Zr} can then capture an electron from the CBM, e.g., previously excited from Dy_{Zr} (or the valence band) to the conduction band, and emits a photon. The peak emission energy related to the optical transition level $E_{\mathrm{opt}}^{0/-}$ (the formation energy difference between $\mathrm{Dy}_\mathrm{Zr}^0$ and the $\mathrm{Dy}_\mathrm{Zr}^-$ configuration in the lattice geometry of $\overline{\mathrm{Dy}_{\mathrm{Zr}}^0}$) is 2.64 eV, with a relaxation energy of 0.43 eV. This indicates that Dy_{Zr} can potentially be the source of a broad blue emission associated with the (nominally) $Dy^{4+} + Zr^{3+} \rightarrow Dy^{3+} + Zr^{4+}$ transition. Further experimental studies are needed to characterize these possible "charge-transfer" transitions (as well as Dy 4f-4f transitions, not considered in this work) in Dy-doped BaZrO₃.

IV. CONCLUSIONS

We have carried out a study of Dy and other relevant defects in BaZrO₃ using hybrid density-functional calculations. We find that Dy has mixed-site occupancy and is stable predominantly as the trivalent Dy³⁺ in the bulk material. The tetravalent Dy⁴⁺ is found to be structurally and electronically stable at the Zr lattice site, but most often energetically less favorable than the trivalent Dy³⁺. This is due to the presence of low-energy, positively charged oxygen vacancies and the mixed-site occupancy of Dy in as-synthesized BaZrO₃. The Dy⁴⁺/Dy³⁺ ratio can, in principle, be increased by preparing the material under highly oxidizing and Ba-rich conditions and co-doping with acceptor-like impurities; however, postsynthesis treatment in oxidizing atmospheres may be needed to realize a non-negligible Dy⁴⁺ concentration. The lattice site preference of Dy (and Y) can also be tuned by tuning the synthesis conditions. Interestingly, we find a strong hybridization between the Dy 4f states and the O 2p states and that the isolated substitutional $\mathrm{Dy_{Zr}}$ defect can be the source of a broad blue emission in band-to-defect luminescence. Our work thus provides a theoretical foundation for understanding experimental observations as well as guidelines for further studies. It also serves as a methodological template for investigating impurities with suspected exotic valence states.

CReDiT AUTHORSHIP STATEMENT

Khang Hoang: Conceptualization, Methodology, Investigation, Visualization, Writing - original draft, Writing - review & editing. Camille Latouche: Resources, Writing - review & editing. Stéphane Jobic: Resources, Writing - review & editing.

ACKNOWLEDGMENTS

K.H. is grateful to Université de Nantes for supporting his visit to Institut des Matériaux Jean Rouxel (IMN) during which this work was initiated. This work used resources of the Center for Computationally Assisted Science and Technology (CCAST) at North Dakota State University, which were made possible in part by NSF MRI Award No. 2019077, and of Centre de Calcul Intensif des Pays de Loire (CCIPL), France.

^[1] McClure DS, Kiss Z. Survey of the Spectra of the Divalent Rare-Earth Ions in Cubic Crystals. J Chem Phys. 1963;39(12):3251-7.

^[2] Kiss ZJ. Energy Levels of Dy²⁺ in the Cubic Hosts of CaF₂, SrF₂, and BaF₂. Phys Rev. 1965;137:A1749-60.

- [3] Joos JJ, Korthout K, Amidani L, Glatzel P, Poelman D, Smet PF. Identification of Dy³⁺/Dy²⁺ as Electron Trap in Persistent Phosphors. Phys Rev Lett. 2020;125:033001.
- [4] Han D, Uda T, Nose Y, Okajima T, Murata H, Tanaka I, et al. Tetravalent Dysprosium in a Perovskite-Type Oxide. Adv Mater. 2012;24(15):2051-3.
- Ricote S, Krishna L, Coors WG, O'Brien JR. Conductivity behavior of BaZr_{0.9}Dy_{0.1}O_{3-δ}. Solid State Ionics. 2018;314:25-9.
- [6] Ricote S, Hudish G, O'Brien JR, Perry NH. Non stoichiometry and lattice expansion of BaZr_{0.9}Dy_{0.1}O_{3-δ} in oxidizing atmospheres. Solid State Ionics. 2019;330:33-9.
- [7] Regalado Vera CY, Ding H, Peterson D, Gibbons WT, Zhou M, Ding D. A mini-review on proton conduction of BaZrO₃-based perovskite electrolytes. J Phys: Energy. 2021;3(3):032019.
- [8] Han D, Shinoda K, Uda T. Dopant Site Occupancy and Chemical Expansion in Rare Earth-Doped Barium Zirconate. J Am Ceram Soc. 2014;97(2):643-50.
- [9] Freysoldt C, Grabowski B, Hickel T, Neugebauer J, Kresse G, Janotti A, et al. First-principles calculations for point defects in solids. Rev Mod Phys. 2014;86:253-305.
- [10] Heyd J, Scuseria GE, Ernzerhof M. Hybrid functionals based on a screened Coulomb potential. J Chem Phys. 2003;118(18):8207-15.
- [11] Hoang K. Hybrid density functional study of optically active Er³⁺ centers in GaN. Phys Status Solidi RRL. 2015;9(12):722-5.
- [12] Hoang K. Tuning the valence and concentration of europium and luminescence centers in GaN through codoping and defect association. Phys Rev Materials. 2021;5:034601.
- [13] Freysoldt C, Neugebauer J, Van de Walle CG. Fully Ab Initio Finite-Size Corrections for Charged-Defect Supercell Calculations. Phys Rev Lett. 2009;102:016402.
- [14] Freysoldt C, Neugebauer J, Van de Walle CG. Electrostatic interactions between charged defects in supercells. phys status solidi (b). 2011;248(5):1067-76.
- [15] Blöchl PE. Projector augmented-wave method. Phys Rev B. 1994;50(24):17953-79.
- [16] Kresse G, Furthmüller J. Efficient iterative schemes for ab initio total-energy calculations using a plane-wave basis set. Phys Rev B. 1996;54(16):11169-86.
- [17] Dudarev SL, Botton GA, Savrasov SY, Humphreys CJ, Sutton AP. Electron-energy-loss spectra and the structural stability of nickel oxide: An LSDA+U study. Phys Rev B. 1998;57(3):1505-9.
- [18] Stull DR, Prophet H. JANAF Thermochemical Tables. 2nd ed. Washington, D.C.: U.S. National Bureau of Standards; 1971.
- [19] Reuter K, Scheffler M. Composition, structure, and stability of RuO₂(110) as a function of oxygen pressure. Phys Rev B. 2001;65:035406.
- [20] Hoang K, Johannes MD. Defect physics in complex energy materials. J Phys: Condens Matter. 2018;30(29):293001.
- [21] Doux JM, Hoang K, Joubert O, Hamon J, Massuyeau F, Quarez E. Ionic to Electronic Transport in

- $Ba_3Ti_3O_6(BO_3)_2$ under Reducing Atmosphere. ACS Appl Energy Mater. 2018;1(2):510-21.
- [22] Yamanaka S, Kurosaki K, Maekawa T, Matsuda T, Kobayashi S, Uno M. Thermochemical and thermophysical properties of alkaline-earth perovskites. J Nucl Mater. 2005;344(1):61-6.
- [23] Borja-Urby R, Diaz-Torres LA, Salas P, Vega-Gonzalez M, Angeles-Chavez C. Blue and red emission in wide band gap BaZrO₃:Yb³⁺,Tm³⁺. Mater Sci Eng B. 2010;174(1):169-73.
- [24] Yuan Y, Zhang X, Liu L, Jiang X, Lv J, Li Z, et al. Synthesis and photocatalytic characterization of a new photocatalyst BaZrO₃. Intl J Hydrogen Energy. 2008;33(21):5941-6.
- [25] Robertson J. Band offsets of wide-band-gap oxides and implications for future electronic devices. J Vac Sci Tech B: Microelectron Nanometer Struct Process Meas Phenom. 2000;18(3):1785-91.
- [26] Gajdoš M, Hummer K, Kresse G, Furthmüller J, Bechstedt F. Linear optical properties in the projector-augmented wave methodology. Phys Rev B. 2006;73:045112.
- [27] Perdew JP, Burke K, Ernzerhof M. Generalized Gradient Approximation Made Simple. Phys Rev Lett. 1996;77(18):3865-8.
- [28] Akbarzadeh AR, Kornev I, Malibert C, Bellaiche L, Kiat JM. Combined theoretical and experimental study of the low-temperature properties of BaZrO₃. Phys Rev B. 2005:72:205104.
- [29] Rowberg AJE, Weston L, Van de Walle CG. Optimizing Proton Conductivity in Zirconates through Defect Engineering. ACS Appl Energy Mater. 2019;2(4):2611-9.
- [30] Knop O, Carlow JS. Revision of the Shannon and Prewitt Effective Ionic Radii of Tetravalent Elements. Can J Chem. 1974;52(12):2175-83.
- [31] Shannon RD. Revised effective ionic radii and systematic studies of interatomic distances in halides and chalcogenides. Acta Crystallogr, Sect A: Found Crystallogr. 1976;32(5):751-67.
- [32] Juhin A, Collins SP, Joly Y, Diaz-Lopez M, Kvashnina K, Glatzel P, et al. Measurement of f orbital hybridization in rare earths through electric dipole-octupole interference in x-ray absorption spectroscopy. Phys Rev Materials. 2019;3:120801.
- [33] Azad AK, Savaniu C, Tao S, Duval S, Holtappels P, Ibberson RM, et al. Structural origins of the differing grain conductivity values in BaZr_{0.9}Y_{0.1}O_{2.95} and indication of novel approach to counter defect association. J Mater Chem. 2008;18:3414-8.
- [34] Yamazaki Y, Hernandez-Sanchez R, Haile SM. Cation non-stoichiometry in yttrium-doped barium zirconate: phase behavior, microstructure, and proton conductivity. J Mater Chem. 2010;20:8158-66.
- [35] Han D, Kishida K, Shinoda K, Inui H, Uda T. A comprehensive understanding of structure and site occupancy of Y in Y-doped BaZrO₃. J Mater Chem A. 2013;1:3027-33.
- [36] Alkauskas A, McCluskey MD, Van de Walle CG. Defects in semiconductors—Combining experiment and theory. J Appl Phys. 2016;119(18):181101.